Isotropy of Cosmic Rays beyond 10^{20} eV Favors Their Heavy Mass Composition

R. U. Abbasi,[1] Y. Abe,[2] T. Abu-Zayyad,[1,3] M. Allen,[3] Y. Arai,[4] R. Arimura,[4] E. Barcikowski,[3] J. W. Belz,[3] D. R. Bergman,[3] S. A. Blake,[3] I. Buckland,[3] B. G. Cheon,[5] M. Chikawa,[6] T. Fujii,[4,30] K. Fujisue,[6,32] K. Fujita,[6] R. Fujiwara,[4] M. Fukushima,[6] G. Furlich,[3] N. Globus,[7,†] R. Gonzalez,[3] W. Hanlon,[3] N. Hayashida,[8] H. He,[7,¶] R. Hibi,[2] K. Hibino,[8] R. Higuchi,[7] K. Honda,[9] D. Ikeda,[8] N. Inoue,[10] T. Ishii,[9] H. Ito,[7] D. Ivanov,[3] A. Iwasaki,[4] H. M. Jeong,[11] S. Jeong,[11] C. C. H. Jui,[3] K. Kadota,[12] F. Kakimoto,[8] O. Kalashev,[13] K. Kasahara,[14] S. Kasami,[15] S. Kawakami,[4] K. Kawata,[6] I. Kharuk,[13] E. Kido,[7] H. B. Kim,[5] J. H. Kim,[3,‡] J. H. Kim,[3] S. W. Kim,[11,**] Y. Kimura,[4] I. Komae,[4] V. Kuzmin,[13,*] M. Kuznetsov,[16,13,§] Y. J. Kwon,[17] K. H. Lee,[11] B. Lubsandorzhiev,[13] J. P. Lundquist,[18,3] H. Matsumiya,[4] T. Matsuyama,[4] J. N. Matthews,[3] R. Mayta,[4] K. Mizuno,[2] M. Murakami,[15] I. Myers,[3] K. H. Lee,[5] S. Nagataki,[7] K. Nakai,[4] T. Nakamura,[19] E. Nishio,[15] T. Nonaka,[6] H. Oda,[4] S. Ogio,[6] M. Onishi,[6] H. Ohoka,[6] N. Okazaki,[6] Y. Oku,[15] T. Okuda,[20] Y. Omura,[4] M. Ono,[7] A. Oshima,[21] H. Oshima,[6] S. Ozawa,[22] I. H. Park,[11] K. Y. Park,[5] M. Potts,[3] M. S. Pshirkov,[13,23] J. Remington,[3,††] D. C. Rodriguez,[3] C. Rott,[3,11] G. I. Rubtsov,[13] D. Ryu,[24] H. Sagawa,[6] R. Saito,[2] N. Sakaki,[6] T. Sako,[6] N. Sakurai,[4] D. Sato,[2] K. Sato,[4] S. Sato,[15] K. Sekino,[6] P. D. Shah,[3] N. Shibata,[15] T. Shibata,[6] J. Shikita,[4] H. Shimodaira,[6] B. K. Shin,[24] H. S. Shin,[4,30] D. Shinto,[15] J. D. Smith,[3] P. Sokolsky,[3] B. T. Stokes,[3] T. A. Stroman,[3] Y. Takagi,[15] K. Takahashi,[6] M. Takamura,[25] M. Takeda,[6] R. Takeishi,[6] A. Taketa,[26] M. Takita,[6] Y. Tameda,[15] K. Tanaka,[27] M. Tanaka,[28] Y. Tanoue,[4] S. B. Thomas,[3] G. B. Thomson,[3] P. Tinyakov,[16,13,‖] I. Tkachev,[13] H. Tokuno,[29] T. Tomida,[2] S. Troitsky,[13] R. Tsuda,[4] Y. Tsunesada,[4,30] S. Udo,[8] F. Urban,[31] D. Warren,[7] T. Wong,[3] K. Yamazaki,[21] K. Yashiro,[25] F. Yoshida,[15] Y. Zhezher,[6,13] and Z. Zundel[3]

(Telescope Array Collaboration)

[1]*Department of Physics, Loyola University Chicago, Chicago, Illinois 60660, USA*
[2]*Academic Assembly School of Science and Technology Institute of Engineering, Shinshu University, Nagano, Nagano 380-8554, Japan*
[3]*High Energy Astrophysics Institute and Department of Physics and Astronomy, University of Utah, Salt Lake City, Utah 84112-0830, USA*
[4]*Graduate School of Science, Osaka Metropolitan University, Sugimoto, Sumiyoshi, Osaka 558-8585, Japan*
[5]*Department of Physics and The Research Institute of Natural Science, Hanyang University, Seongdong-gu, Seoul 426-791, Korea*
[6]*Institute for Cosmic Ray Research, University of Tokyo, Kashiwa, Chiba 277-8582, Japan*
[7]*Astrophysical Big Bang Laboratory, RIKEN, Wako, Saitama 351-0198, Japan*
[8]*Faculty of Engineering, Kanagawa University, Yokohama, Kanagawa 221-8686, Japan*
[9]*Interdisciplinary Graduate School of Medicine and Engineering, University of Yamanashi, Kofu, Yamanashi 400-8511, Japan*
[10]*The Graduate School of Science and Engineering, Saitama University, Saitama, Saitama 338-8570, Japan*
[11]*Department of Physics, SungKyunKwan University, Jang-an-gu, Suwon 16419, Korea*
[12]*Department of Physics, Tokyo City University, Setagaya-ku, Tokyo 158-8557, Japan*
[13]*Institute for Nuclear Research of the Russian Academy of Sciences, Moscow 117312, Russia*
[14]*Faculty of Systems Engineering and Science, Shibaura Institute of Technology, Minato-ku, Tokyo 337-8570, Japan*
[15]*Graduate School of Engineering, Osaka Electro-Communication University, Hatsu-cho, Neyagawa-shi, Osaka 572-8530, Japan*
[16]*Service de Physique Théorique, Université Libre de Bruxelles, Brussels 1050, Belgium*
[17]*Department of Physics, Yonsei University, Seodaemun-gu, Seoul 120-749, Korea*

[†]Present address: KIPAC, Stanford University, Stanford, CA 94305, USA.
[¶]Present address: Purple Mountain Observatory, Nanjing 210023, China.
[‡]Present address: Physics Department, Brookhaven National Laboratory, Upton, NY 11973, USA.
[**]Present address: Korea Institute of Geoscience and Mineral Resources, Daejeon, 34132, Korea.
[*]Deceased.
[§]mkuzn@inr.ac.ru
[††]Present address: NASA Marshall Space Flight Center, Huntsville, Alabama 35812 USA.
[‖]petr.tiniakov@ulb.be

[18]Center for Astrophysics and Cosmology, University of Nova Gorica, Nova Gorica 5297, Slovenia
[19]Faculty of Science, Kochi University, Kochi, Kochi 780-8520, Japan
[20]Department of Physical Sciences, Ritsumeikan University, Kusatsu, Shiga 525-8577, Japan
[21]College of Engineering, Chubu University, Kasugai, Aichi 487-8501, Japan
[22]Quantum ICT Advanced Development Center, National Institute for Information and Communications Technology, Koganei, Tokyo 184-8795, Japan
[23]Sternberg Astronomical Institute, Moscow M.V. Lomonosov State University, Moscow 119991, Russia
[24]Department of Physics, School of Natural Sciences, Ulsan National Institute of Science and Technology, UNIST-gil, Ulsan 689-798, Korea
[25]Department of Physics, Tokyo University of Science, Noda, Chiba 162-8601, Japan
[26]Earthquake Research Institute, University of Tokyo, Bunkyo-ku, Tokyo 277-8582, Japan
[27]Graduate School of Information Sciences, Hiroshima City University, Hiroshima, Hiroshima 731-3194, Japan
[28]Institute of Particle and Nuclear Studies, KEK, Tsukuba, Ibaraki 305-0801, Japan
[29]Graduate School of Science and Engineering, Tokyo Institute of Technology, Meguro, Tokyo 152-8550, Japan
[30]Nambu Yoichiro Institute of Theoretical and Experimental Physics, Osaka Metropolitan University, Sugimoto, Sumiyoshi, Osaka 558-8585, Japan
[31]CEICO, Institute of Physics, Czech Academy of Sciences, Prague 182 21, Czech Republic
[32]Institute of Physics, Academia Sinica, Taipei City 115201, Taiwan

(Received 24 March 2023; revised 15 April 2024; accepted 21 May 2024; published 22 July 2024)

We report an estimation of the injected mass composition of ultrahigh energy cosmic rays (UHECRs) at energies higher than 10 EeV. The composition is inferred from an energy-dependent sky distribution of UHECR events observed by the Telescope Array surface detector by comparing it to the Large Scale Structure of the local Universe. In the case of negligible extragalactic magnetic fields (EGMFs), the results are consistent with a relatively heavy injected composition at $E \sim 10$ EeV that becomes lighter up to $E \sim 100$ EeV, while the composition at $E > 100$ EeV is very heavy. The latter is true even in the presence of highest experimentally allowed extragalactic magnetic fields, while the composition at lower energies can be light if a strong EGMF is present. The effect of the uncertainty in the galactic magnetic field on these results is subdominant.

DOI: 10.1103/PhysRevLett.133.041001

Ultrahigh energy cosmic rays (UHECR) are charged particles, likely protons and nuclei, with energies greater than 1 EeV (10^{18} eV) that are reaching Earth from space. The flux of particles at these energies is tiny, of order 1 $\mathrm{km^{-2}\,sr^{-1}\,yr^{-1}}$, so they can be detected only indirectly via extensive air showers (EAS) of secondary particles they initiate in Earth's atmosphere. Despite several decades of study, the origin of UHECR and the nature of their primary particles remain unknown. The UHECR energy spectrum was measured with a good precision [1,2]; its general shape is consistent between the two modern experiments Pierre Auger (Auger) [3] and Telescope Array (TA) [4] and with theoretical models [5–7], except for a minor discrepancy [8] at highest energies. The spectrum measurements alone, however, have a limited potential to discriminate between various models of UHECR origin. The mass composition measurements have generally better discriminating power. But opposite to the spectrum, the mass composition measurements of Auger [9,10] and TA [11,12] are more affected by various systematic effects and not covering the highest energy part of the UHECR spectrum. At the same time the UHECR arrival directions are measured with a sufficient precision of order 1°. Unfortunately, this does not allow one to directly identify the sources since the deflections of UHECR are highly uncertain because of both unknown event-by-event primary particle charges and because of large uncertainties in the galactic and extragalactic magnetic fields. Several approaches have been proposed in the literature to decipher the origin of UHECR using complex anisotropy observables [13–16].

In this Letter we use a novel method to infer the *injected* UHECR mass composition from the arrival directions of the TA events. The method was proposed and described in detail in Ref. [17]. It takes advantage of the accurate measurements of UHECR arrival directions and energy, while circumventing the uncertainties arising from cosmic magnetic fields. The method is based on the observation that the magnitude of UHECR deflections is determined predominantly by particle charges that may range from 1 for protons to 26 for iron, while other factors are expected to give an order of magnitude smaller effect. Comparing the energy-dependent UHECR distribution over the sky calculated with various injected mass compositions with the observed distribution, one may identify the models that are compatible or incompatible with the data. At this stage, the parameters of the UHECR models other than the mass composition are fixed by some conservative assumptions. One may then vary these parameters to check if the

conclusions about the mass composition are robust with respect to this variation. Somewhat similar approaches to UHECR mass composition estimation from their anisotropy have been proposed in Refs. [18,19].

The Telescope Array [4] is the largest cosmic-ray experiment in the Northern Hemisphere. It is located at 39.3° N, 112.9° W in Utah, USA. The observatory includes a surface detector array (SD) and 38 fluorescence telescopes grouped in three stations. The SD consists of 507 plastic scintillator stations of 3 m^2 each, which are placed in a square grid with the 1.2 km spacing, covering in total the area of $\sim 700\ km^2$. The TA SD can detect EAS produced by cosmic ray particles of ∼EeV and higher energies. The TA SD has been in operation since May 2008. In this analysis we use the data collected by the TA SD during 14 years of operation from May 11, 2008 to May 10, 2022. We use the quality cuts described in Ref. [20], and select events with zenith angle $\theta < 55°$ and energy $E > 10$ EeV. We also use the data of the National Lightning Detection Network [21] to filter out the events possibly caused by lightnings as described in Ref. [22]. The resulting dataset contains 5978 events, including the event with the highest energy of 244 EeV [23] and 18 other events with $E > 100$ EeV.

Each event that activates the SD trigger is recorded, and the kinematic parameters of its primary particle are reconstructed. The arrival direction is determined from the relative difference in arrival times of the shower front at each surface detector, which is measured with the precision of 20 ns. The energy of the primary particle is estimated using the EAS particle density S_{800} measured at a distance of 800 m from the shower axis. The measured value of S_{800} is converted to the reconstructed SD energy taking into account the zenith angle dependence by means of a Monte Carlo simulation that uses the CORSIKA software package [24]. Finally, thus reconstructed SD energy is calibrated to the calorimetric energy measured by the fluorescence detectors; this amounts to a rescaling by the factor of $1/1.27$ [2]. The resolution of the SD at $E > 10$ EeV is 1.4° in arrival direction and 18% in the logarithm of primary energy [2,25]. The systematic uncertainty in the energy determination is estimated at 21% [26].

The implementation of our method is organized in three steps. First, we generate a large mock set of realistic UHECR events for each injected composition model considered. Second, we define the test statistics (TS) that quantify the overall magnitude of deflections of a given event set with respect to the large scale structure (LSS) of the Universe and that is robust to the uncertainties of the magnetic fields. Finally, we calculate this TS for each mock event set as well as for the real data, and quantify the compatibility of each composition model with the data. The effect of the uncertainties in magnetic fields and injection spectra is estimated by varying their parameters for each composition model.

We now describe these steps in more detail, starting with a brief description of the key properties of the UHECR mock event sets; more thorough discussion is given in a companion paper [27]. We assume that UHECR sources trace the matter distribution in the local Universe. Statistically, this can be achieved by assuming equal intrinsic UHECR flux for each galaxy in a complete volume-limited sample. In practice we use the flux-limited galaxy sample with a high degree of completeness, derived from the 2MRS galaxy catalog [28] by cutting out galaxies with mag > 12.5 and with distances below 5 Mpc and beyond 250 Mpc. We assign a progressively larger flux to more distant galaxies to compensate for the observational selection inherent in a flux-limited sample. The sources beyond 250 Mpc are assumed to be distributed uniformly with the same mean density as those within this distance. Their contribution is added as a properly normalized fraction of isotropic events. The exact procedure is described in Ref. [29]. This source model covers all the source scenarios with sufficiently numerous sources (source number density $\rho \gg 10^{-5}\ \mathrm{Mpc}^{-3}$). The source densities of order $10^{-5}\ \mathrm{Mpc}^{-3}$ are not excluded experimentally [30] (see, however, recent studies [31,32]). In this case the sensitivity of our method to the mass composition decreases; we discuss this issue in a companion paper [27].

We fix the injection spectrum for each nucleus by deriving it from the separate fit to the TA and Auger observed spectra [27,33]. As a result the following spectra are taken for the UHECR flux simulation: power law with the slope −2.55, −2.20, −2.10 and without the cutoff for protons, helium, and oxygen, respectively; power law with the slope −1.50 and with a sharp cutoff at 280 EeV for silicon; and power law with the slope −1.95 and with a sharp cutoff at 560 EeV for iron. The secondary particles produced upon propagation of injected primary nuclei through the interstellar medium are taken into account for helium and oxygen nuclei and reasonably neglected for other primaries; the details are given in Ref. [33]. We also consider separately a best-fit injected composition model from the Auger work [34], where we take into account all the secondaries and model the deflection of the full flux according to its average charge.

The deflections in magnetic fields are treated with the account of primary particle charge Z and its energy E. The deflections in the extragalactic magnetic field (EGMF) are simulated as a direction-independent smearing of the sources with the von Mises-Fischer distribution. For our basic model its magnitude is set to zero, which corresponds to either $B_{\mathrm{EGMF}} \ll 1$ nG for the correlation length $\lambda \sim 1$ Mpc or $B_{\mathrm{EGMF}} \ll 0.1$ nG for λ of a cosmological scale. We discuss the possible effect of nonzero EGMF among other uncertainties. The deflections in the regular galactic magnetic field (GMF) are simulated using the backtracking technique with the GMF model of Ref. [35]. The deflections in the random GMF are

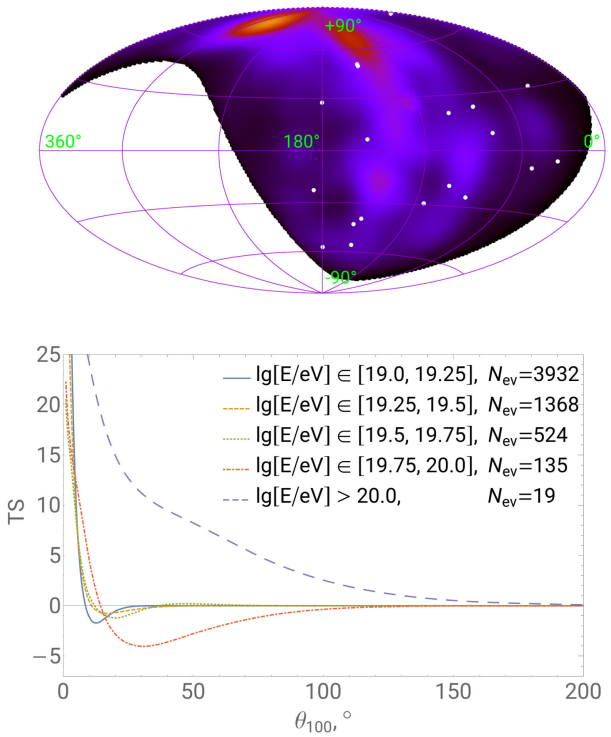

FIG. 1. Top: example of the map Φ_k ($E > 100$ EeV, $\theta_{100} = 10°$) used for test-statistics computation, overlaid with the distribution of the TA SD events with $E > 100$ EeV (two of them are forming a doublet). The color indicates the expected distribution of the cosmic ray flux. Galactic coordinates. Bottom: distribution of test statistics over θ_{100} evaluated for experimental data in five energy bins. The number of events in each bin is shown in the legend.

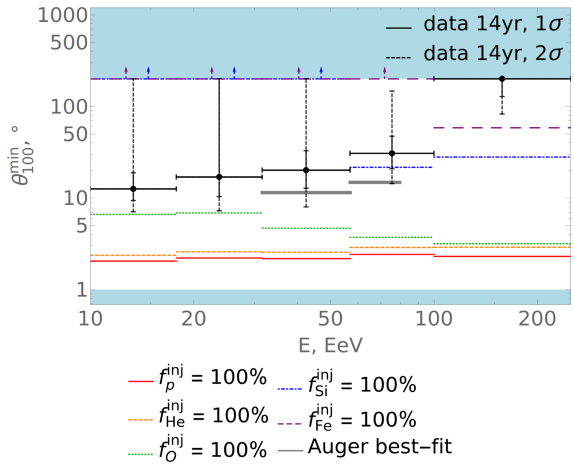

FIG. 2. The distribution of the test-statistics minima, $\theta_{100}^{\min}$, for the data compared to several injected composition models. Regular GMF model of Ref. [35] is used, and deflections in EGMF are neglected. Note that several heavy composition models yield the same value of $\theta_{100}^{\min} = 200°$, i.e. they are indistinguishable in our method. The corresponding lines which merge together on the plot are indicated by arrows. Pure nuclei composition models and Auger composition model of Ref. [34] (see text).

simulated as a galactic-latitude-dependent smearing according to the data-driven relation of Ref. [36]. Finally, the event distribution is modulated by the geometrical exposure of the TA. The energies of the events in the mock sets are generated according to the observed TA spectrum with the account of the TA energy resolution. In a companion paper [27] we estimate the impact of uncertainties in the energy scale and in the parameters of the injection spectra and magnetic fields on the inferred mass composition.

We define the test statistics using the expected UHECR flux maps built by a similar procedure as used for the mock sets generation, but with smaller number of free parameters. Namely, we use the same 2MRS-based source catalog, assume flux attenuation as protons with $\sim E^{-2.55}$ injection spectrum without cutoff and a uniform smearing of sources. The magnitude of this smearing θ_{100} defined at 100 EeV is the only free parameter on which the TS depends. For each given value of θ_{100} we build a set of maps $\Phi_k(\theta_{100}, \mathbf{n})$ where $\mathbf{n}$ is the direction in the sky, k denotes the energy bin and the smearing of each map scales properly, as 100 EeV$/E_k$. Then the test statistics $\mathrm{TS}(\theta_{100})$ for a given event set with directions $\mathbf{n}_i$ is defined as follows:

$$\mathrm{TS}(\theta_{100}) = -2\sum_k \left(\sum_i \ln \frac{\Phi_k(\theta_{100}, \mathbf{n}_i)}{\Phi_{\mathrm{iso}}(\mathbf{n}_i)} \right), \qquad (1)$$

where the sum run over the events i and energy bins k, and we have included a standard overall normalization factor -2. The normalization factor $\Phi_{\mathrm{iso}}(\mathbf{n}_i) = \Phi(\infty, \mathbf{n}_i)$ corresponding to an isotropic distribution is added for convenience. More technical details on the TS construction are given in the companion paper [27]. In the limit of a large number of events, this test statistics is distributed around its minimum according to χ^2 distribution with one degree of freedom. The position of the TS minimum $\theta_{100}^{\min}$ for each event set is interpreted as the energy-rescaled mean event deflection with respect to the LSS. Thus, for a mock set of a given composition model and a very large number of events, the TS should have a deep and narrow minimum, with the value of $\theta_{100}^{\min}$ being characteristic of this composition model. These values could then be confronted with the $\mathrm{TS}(\theta_{100})$ evaluated for the data.

To estimate the mass composition we divide the energy range into five bins starting from 10 EeV with a quarter-decade width and with the last bin being an open interval $E > 100$ EeV. The dependence of $\mathrm{TS}(\theta_{100})$ on θ_{100} for the data in each bin is shown in Fig. 1. The curves for all but the penultimate bin (red curve) are consistent, at the 2σ level, with isotropy which corresponds to $\theta_{100} = 200°$ in our notations—the value that is beyond the size of the TA field of view. In the bin $19.75 < \log_{10}[E/\mathrm{eV}] < 20.0$ the TS has a distinct minimum at $\theta_{100}^{\min} = 30.8°$ that deviates from isotropy with the significance of more than 2σ.

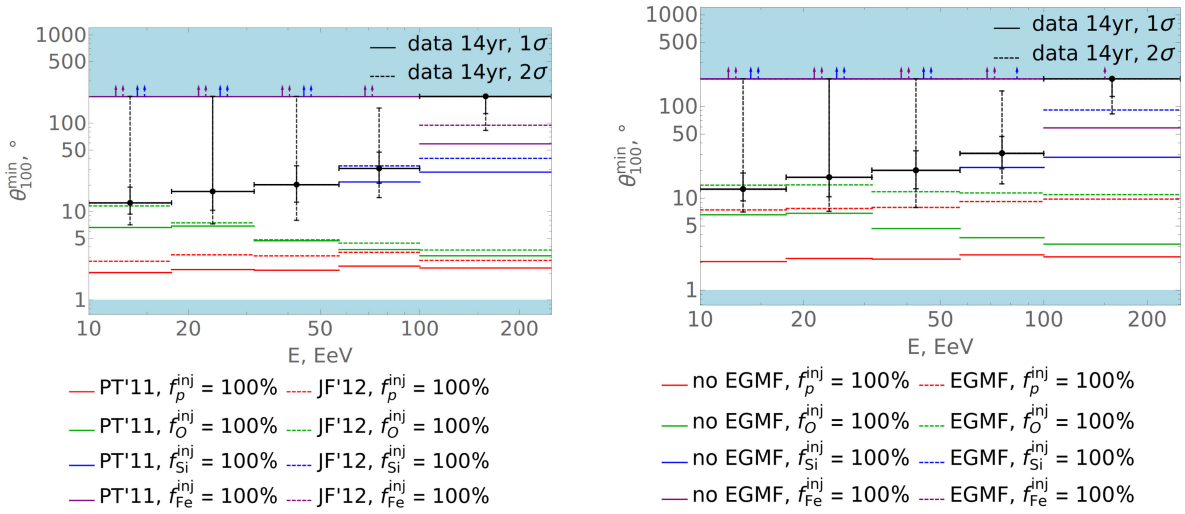

FIG. 3. Test statistics for the data compared to various pure nuclei injected composition models. Left: results for two different regular GMF models. Right: results without EGMF and with extremely strong EGMF.

In Fig. 2 we present a bin-wise comparison of the data with various composition models. The data points are in correspondence with the TS(θ_{100}) curves shown in Fig. 1: the central points show values of $\theta_{100}^{\rm min}$ in each bin, while the error bars represent 1σ and 2σ deviations from the minimum as calculated from the corresponding curve. It should be stressed that, by definition, the data points show typical deflections of cosmic rays in the corresponding bin *rescaled to* $E = 100$ EeV. While the energy dependence of deflections is taken into account in this way, the other factors such as the difference in attenuation at different energies (and, therefore, relative contribution of close and distant sources) are not. Hence the variations of $\theta_{100}^{\rm min}$ from bin to bin. Regardless these variations, it is manifest in Fig. 2 that the small values of θ_{100} are not compatible with the data at all energies, which is evident already in Fig. 1 from the steep rise of the curves at small θ_{100}.

The colored lines in Fig. 2 show predictions for different composition models which should be compared to the data. With our assumptions and zero EGMF the pure proton composition (red line) is not compatible with the data as it predicts $\theta_{100}^{\rm min} \lesssim 2°$ in all energy bins. The injected light or intermediate composition is also incompatible with the data as in this case the flux is dominated by secondary protons. At the same time the data are compatible with the injected silicon at all energies except $E > 100$ EeV and with injected iron at all energies except $E \gtrsim 56$ EeV. The Auger best-fit model is compatible with the data at 2σ level.

In general, one can see a trend: the preference for heavier composition at $10 < E \lesssim 18$ EeV changes in favor of a lighter one at $56 \lesssim E < 100$ EeV, while at $E > 100$ EeV the data prefer a very heavy composition—even beyond iron.

We turn now to the discussion of uncertainties affecting these results, of which the most important are those related to the magnetic fields, the experimental energy scale and the injection spectrum. In our setup all these uncertainties affect only the positions of model lines shown in Fig. 2. The injection spectrum uncertainty was tested by varying the spectrum parameters within $\pm 1\sigma$ around their best-fit values. This variation was found to have negligible impact on the results, see Ref. [27] for details.

To estimate the effect of GMF uncertainty we generate new mock sets, this time assuming the regular GMF model of Ref. [37]. Note that the UHECR deflections in both models are similar in magnitude but substantially differ in direction. The comparison of predicted values of $\theta_{100}^{\rm min}$ is shown in Fig. 3, left panel, for the same composition models as in Fig. 2. One can see that the predicted values of $\theta_{100}^{\rm min}$ are quite close in almost all cases, so that the change of the GMF model does not change the level of compatibility of the composition models with the data.

The EGMF is more uncertain than GMF. To estimate its impact on the results, additional assumptions are required. In general, there are three possible regimes where EGMF may affect the UHECR deflections. First, there could be an intergalactic magnetic field *IGMF* in voids of the large-scale structure. If its origin is not cosmological its correlation length is expected not to exceed ~1 Mpc [38]. Then its strength is bounded from above as $B_{\rm EGMF} < 1.7$ nG [39] and UHECR deflections are described by a uniform smearing [40]. It is straightforward to implement such a smearing into our simulation of mock sets. In the opposite case of the IGMF of cosmological origin, its amplitude is constrained to be $B \lesssim 0.05$ nG for any correlation lengths [41], that leads to deflections negligible comparing to that in the GMF. Finally, the IGMF can be negligible but there could be an EGMF in a local extragalctic structure such as a local filament. There is no observational bounds on such fields; however, constrained astrophysical simulations predict its strength in the range $0.3 < B < 3$ nG in the ~5 Mpc vicinity of our Galaxy [42]. Even in the conservative case the expected deflections in such a field

would be several times smaller than the maximum possible deflections in IGMF.

Given all these considerations we test the possible effect of EGMF conservatively assuming the highest allowed parameters for a noncosmological field [39]: $B_{\mathrm{EGMF}} = 1.7$ nG and $\lambda_{\mathrm{EGMF}} = 1$ Mpc. This may lead to deflections as high as 7° for protons at 100 EeV. We are simulating such deflections by an additional direction-independent smearing of sources that scales according to the primary particle charge and energy. The results including both GMF and EGMF are shown in Fig. 3, right panel, in comparison with the zero EGMF case. As one can see from the plot, the inclusion of the maximum allowed EGMF significantly increases the value of $\theta_{100}^{\mathrm{min}}$ in all models and makes even the pure proton composition compatible with the data in lower energy bins at the 2σ level. In the last bin corresponding to $E > 100$ EeV, this increase is not sufficient except in the case of pure iron composition which becomes fully compatible with the data.

The impact of the uncertainty related to the systematic uncertainty of the experiment's energy scale is of the same order or smaller than the impact of the GMF uncertainty. More detailed discussion of all the mentioned uncertainties is given in Ref. [27].

The interpretation of the results differs significantly depending on the assumed deflections in EGMF, while the difference due to the GMF assumptions is subdominant. As it was mentioned, in the case of negligible EGMF the data prefer a heavy composition at low energies, a relatively light one at $56 \lesssim E < 100$ EeV, and a very heavy one (beyond iron) at $E > 100$ EeV. The latter result is in agreement with Ref. [23], which finds that the TA highest energy event is not correlated with the LSS unless its deflection is very large. In the case of extreme EGMF the data is consistent with both heavy and intermediate composition at $E < 100$ EeV. In particular oxygen and even proton compositions became more compatible with the data at $E \lesssim 56$ EeV.

Importantly, the evidence of heavy composition at $E > 100$ EeV survives the assumption of even extremely strong EGMF, while the light or intermediate composition remains in tension with the data. For instance, to reconcile the proton or helium composition with the data at $E > 100$ EeV at least at the 2σ level the EGMF should be stronger than 20 nG for $\lambda = 1$ Mpc, that is far beyond the upper limit discussed earlier. It is also interesting that pure silicon is compatible with data from 10 EeV up to 100 EeV irrespective of the EGMF.

In conclusion, an important comment concerning the interpretation of our results in the low-energy bins is in order. The logic here can be inverted: taking at face value the light or intermediate composition measured at $10 \lesssim E \lesssim 50$ EeV by the fluorescence experiments [9,11], our results implying relatively large UHECR deflections at these energies point toward the existence of a strong EGMF close to the current experimental limit. The quantitative discussion of this observation will be given elsewhere.

Acknowledgments—The authors would like to thank the former member of the Telescope Array collaboration Armando di Matteo, who kindly provided the simulations of UHECR propagation and respective fits of attenuation curves for the purposes of this study. The Telescope Array experiment is supported by the Japan Society for the Promotion of Science (JSPS) through Grants-in-Aid for Priority Area 431, for Specially Promoted Research JP21000002, for Scientific Research (S) JP19104006, for Specially Promoted Research JP15H05693, for Scientific Research (S) JP19H05607, for Scientific Research (S) JP15H05741, for Science Research (A) JP18H03705, for Young Scientists (A) JPH26707011, and for Fostering Joint International Research (B) JP19KK0074, by the joint research program of the Institute for Cosmic Ray Research (ICRR), The University of Tokyo; by the Pioneering Program of RIKEN for the Evolution of Matter in the Universe (r-EMU); by the U.S. National Science Foundation Awards No. PHY-1806797, No. PHY-2012934, No. PHY-2112904, No. PHY-2209583, No. PHY-2209584, and No. PHY-2310163, as well as No. AGS-1613260, No. AGS-1844306, and No. AGS-2112709; by the National Research Foundation of Korea (2017K1A4A3015188, 2020R1A2C1008230, and 2020R1A2C2102800); by the Ministry of Science and Higher Education of the Russian Federation under Contract No. 075-15-2024-541, IISN Project No. 4.4501.18, by the Belgian Science Policy under IUAP VII/37 (ULB) by the European Union and Czech Ministry of Education, Youth and Sports through the FORTE Project No. CZ.02.01.01/00/22_008/0004632, and by the Simons Foundation (00001470, NG). This work was partially supported by the grants of the joint research program of the Institute for Space-Earth Environmental Research, Nagoya University and Inter-University Research Program of the Institute for Cosmic Ray Research of University of Tokyo. The foundations of Dr. Ezekiel R. and Edna Wattis Dumke, Willard L. Eccles, and George S. and Dolores Doré Eccles all helped with generous donations. The State of Utah supported the project through its Economic Development Board, and the University of Utah through the Office of the Vice President for Research. The experimental site became available through the cooperation of the Utah School and Institutional Trust Lands Administration (SITLA), U.S. Bureau of Land Management (BLM), and the U.S. Air Force. We appreciate the assistance of the State of Utah and Fillmore offices of the BLM in crafting the Plan of Development for the site. We thank Patrick A. Shea who assisted the collaboration with valuable advice and supported the collaboration's efforts. We gratefully acknowledge the contribution from the technical staffs of our home institutions. An allocation of computing resources from the Center for High Performance Computing at the University of Utah as well as the Academia Sinica Grid Computing Center (ASGC) is gratefully acknowledged.

[1] J. Abraham *et al.* (Pierre Auger Collaboration), Measurement of the energy spectrum of cosmic rays above 10^{18} eV using the Pierre Auger observatory, Phys. Lett. B **685**, 239 (2010).

[2] T. Abu-Zayyad *et al.* (Telescope Array Collaboration), The cosmic ray energy spectrum observed with the surface detector of the Telescope Array experiment, Astrophys. J. **768**, L1 (2013).

[3] A. Aab *et al.* (Pierre Auger Collaboration), The Pierre Auger cosmic ray observatory, Nucl. Instrum. Methods Phys. Res., Sect. A **798**, 172 (2015).

[4] T. Abu-Zayyad *et al.* (Telescope Array Collaboration), The surface detector array of the Telescope Array experiment, Nucl. Instrum. Methods Phys. Res., Sect. A **689**, 87 (2013).

[5] K. Greisen, End to the cosmic ray spectrum?, Phys. Rev. Lett. **16**, 748 (1966).

[6] G. T. Zatsepin and V. A. Kuzmin, Upper limit of the spectrum of cosmic rays, JETP Lett. **4**, 78 (1966).

[7] R. Aloisio, V. Berezinsky, and A. Gazizov, Ultra high energy cosmic rays: The disappointing model, Astropart. Phys. **34**, 620 (2011).

[8] R. Abbasi *et al.* (Telescope Array and Pierre Auger Collaborations), Joint analysis of the energy spectrum of ultra-high-energy cosmic rays as measured at the Pierre Auger observatory and the Telescope Array, Proc. Sci., ICRC2021 (**2021**) 337.

[9] A. Aab *et al.* (Pierre Auger Collaboration), Depth of maximum of air-shower profiles at the Pierre Auger observatory. II. Composition implications, Phys. Rev. D **90**, 122006 (2014).

[10] A. Aab *et al.* (Pierre Auger Collaboration), Inferences on mass composition and tests of hadronic interactions from 0.3 to 100 EeV using the water-Cherenkov detectors of the Pierre Auger observatory, Phys. Rev. D **96**, 122003 (2017).

[11] R. U. Abbasi *et al.* (Telescope Array Collaboration), Depth of ultra high energy cosmic ray induced air shower maxima measured by the Telescope Array black rock and long ridge FADC fluorescence detectors and surface array in hybrid mode, Astrophys. J. **858**, 76 (2018).

[12] R. U. Abbasi *et al.* (Telescope Array Collaboration), Mass composition of ultrahigh-energy cosmic rays with the Telescope Array surface detector data, Phys. Rev. D **99**, 022002 (2019).

[13] O. Kalashev, M. Pshirkov, and M. Zotov, Identifying nearby sources of ultra-high-energy cosmic rays with deep learning, J. Cosmol. Astropart. Phys. 11 (2020) 005.

[14] F. R. Urban, S. Camera, and D. Alonso, Detecting ultra-high-energy cosmic ray anisotropies through harmonic cross-correlations, Astron. Astrophys. **652**, A41 (2021).

[15] T. Bister, M. Erdmann, J. Glombitza, N. Langner, J. Schulte, and M. Wirtz, Identification of patterns in cosmic-ray arrival directions using dynamic graph convolutional neural networks, Astropart. Phys. **126**, 102527 (2021).

[16] R. U. Abbasi *et al.* (Telescope Array Collaboration), Evidence for a supergalactic structure of magnetic deflection multiplets of ultra-high energy cosmic rays, Astrophys. J. **899**, 86 (2020).

[17] M. Y. Kuznetsov and P. G. Tinyakov, UHECR mass composition at highest energies from anisotropy of their arrival directions, J. Cosmol. Astropart. Phys. 04 (2021) 065.

[18] R. C. dos Anjos *et al.*, Ultrahigh-energy cosmic ray composition from the distribution of arrival directions, Phys. Rev. D **98**, 123018 (2018).

[19] K. Tanidis, F. R. Urban, and S. Camera, Constraining ultra-high-energy cosmic ray composition through cross-correlations, J. Cosmol. Astropart. Phys. 12 (2022) 003.

[20] A. Aab *et al.* (Telescope Array and Pierre Auger Collaborations), Searches for large-scale anisotropy in the arrival directions of cosmic rays detected above energy of 10^{19} eV at the Pierre Auger observatory and the Telescope Array, Astrophys. J. **794**, 172 (2014).

[21] K. Cummins and M. J. Murphy, An overview of lightning locating systems: History, techniques, and data uses, with an in-depth look at the U.S. NLDN, IEEE Trans. **51**, 499 (2009).

[22] R. U. Abbasi *et al.* (Telescope Array Collaboration), Constraints on the diffuse photon flux with energies above 10^{18} eV using the surface detector of the Telescope Array experiment, Astropart. Phys. **110**, 8 (2019).

[23] R. U. Abbasi *et al.* (Telescope Array Collaboration), An extremely energetic cosmic ray observed by a surface detector array, Science **382**, abo5095 (2023).

[24] D. Heck, J. Knapp, J. N. Capdevielle, G. Schatz, and T. Thouw, CORSIKA: A Monte Carlo code to simulate extensive air showers, Universität Karlsruhe, Karlsruhe, Germany, Report No. FZKA-6019, 1998.

[25] Telescope Array Collaboration, CORSIKA simulation of the telescope array surface detector, arXiv:1403.0644.

[26] R. U. Abbasi *et al.* (Telescope Array Collaboration), The energy spectrum of cosmic rays above $10^{17.2}$ eV measured by the fluorescence detectors of the Telescope Array experiment in seven years, Astropart. Phys. **80**, 131 (2016).

[27] R. U. Abbasi *et al.* (Telescope Array Collaboration), companion paper, Phys. Rev. D **110**, 022006 (2024).

[28] J. P. Huchra *et al.*, The 2 MASS redshift survey: Description and data release, Astrophys. J. Suppl. Ser. **199**, 26 (2012).

[29] H. B. Koers and P. Tinyakov, Flux calculations in an inhomogeneous Universe: Weighting a flux-limited galaxy sample, Mon. Not. R. Astron. Soc. **399**, 1005 (2009).

[30] P. Abreu *et al.* (Pierre Auger Collaboration), Bounds on the density of sources of ultra-high energy cosmic rays from the Pierre Auger observatory, J. Cosmol. Astropart. Phys. 05 (2013) 009.

[31] M. Y. Kuznetsov, A nearby source of ultra-high energy cosmic rays, J. Cosmol. Astropart. Phys. 04 (2024) 042.

[32] T. Bister and G. R. Farrar, Constraints on UHECR sources and extragalactic magnetic fields from directional anisotropies, Astrophys. J. **966**, 71 (2024).

[33] A. di Matteo and P. Tinyakov, How isotropic can the UHECR flux be?, Mon. Not. R. Astron. Soc. **476**, 715 (2018).

[34] A. Aab *et al.* (Pierre Auger Collaboration), Combined fit of spectrum and composition data as measured by the Pierre Auger observatory, J. Cosmol. Astropart. Phys. 04 (2017) 038; 03 (2018) E02.

[35] M. S. Pshirkov, P. G. Tinyakov, P. P. Kronberg, and K. J. Newton-McGee, Deriving global structure of the galactic magnetic field from faraday rotation measures of extragalactic sources, Astrophys. J. **738**, 192 (2011).
[36] M. S. Pshirkov, P. G. Tinyakov, and F. R. Urban, Mapping UHECRs deflections through the turbulent galactic magnetic field with the latest RM data, Mon. Not. R. Astron. Soc. **436**, 2326 (2013).
[37] R. Jansson and G. R. Farrar, A new model of the galactic magnetic field, Astrophys. J. **757**, 14 (2012).
[38] R. Durrer and A. Neronov, Cosmological magnetic fields: Their generation, evolution and observation, Astron. Astrophys. Rev. **21**, 62 (2013).
[39] M. Pshirkov, P. Tinyakov, and F. Urban, New limits on extragalactic magnetic fields from rotation measures, Phys. Rev. Lett. **116**, 191302 (2016).
[40] P. Bhattacharjee and G. Sigl, Origin and propagation of extremely high-energy cosmic rays, Phys. Rep. **327**, 109 (2000).
[41] K. Jedamzik and A. Saveliev, Stringent limit on primordial magnetic fields from the cosmic microwave background radiation, Phys. Rev. Lett. **123**, 021301 (2019).
[42] S. Hackstein, F. Vazza, M. Brüggen, J. G. Sorce, and S. Gottlöber, Simulations of ultra-high energy cosmic rays in the local universe and the origin of cosmic magnetic fields, Mon. Not. R. Astron. Soc. **475**, 2519 (2018).